Modeling and observation of heat losses from buildings: The impact of geometric detail on 3D heat flux modeling

Danbi Lee[1], Peter Pietrzyk[1], Sjors Donkers[1], Vera Liem[1], Jelte van Oostveen[1], Sina Montazeri[1], Roeland Boeters[1], Jerome Colin[2], Pierre Kastendeuch[2], Françoise Nerry[2], Massimo Menenti[3], Ben Gorte[3] and Edward Verbree[4]

[1] Delft University of Technology, Netherlands, MSc. Geomatics; d.j.lee@student.tudelft.nl, p.j.pietrzyk@student.tudelft.nl, s.donkers@student.tudelft.nl, v.c.g.liem@student.tudelft.nl, j.g.vanOostveen@student.tudelft.nl, s.montazeri@student.tudelft.nl, r.boeters@student.tudelft.nl

[2] University of Strasbourg, ICube Laboratory, Strasbourg, France; j.colin@unistra.fr, kasten@unistra.fr, f.nerry@unistra.fr

[3] Delft University of Technology, Geosciences and Remote Sensing, Delft, Netherlands; m.menenti@tudelft.nl, b.g.h.gorte@tudelft.nl

[4]Delft University of Technology, OTB Research Institute for the Built Environment, Delft, Netherlands: e.verbree@tudelft.nl

Abstract. The impact of 3D geometry complexity on the accuracy of simulating radiative, convective and conductive fluxes in an urban canyon was explored. The research involved the collection of meteorological data in an urban canyon in the city of Strasbourg, France, for input into a 3D model called LASER/F, which simulates the aforementioned fluxes. The key input into LASER/F is a 3D geometric model representing the scene (urban canyon). It was hypothesized that more geometric detail in the model would lead to improved accuracy in the simulation but increased computing time. To test this, seven geometry scenarios were prepared with different complexities and test run in LASER/F. The results were validated with thermal images of two facades collected during the field campaign in Strasbourg. The results show that LASER/F systematically underestimates facade surface temperatures possibly due to various model assumptions and input geometry. One of those is the oversimplified 1D parameterization of the vertical wind profile and was demonstrated by comparing it with a vertical wind profile extracted from a CFD model. It was concluded that the most complex 3D geometry does not necessarily improve simulation accuracy, especially during warming periods of the day, but does affect simulation time. The inclusion of balconies on the facades is influential and should be used for future simulation experiments when it is a significant feature of a facade. This implies that 3D simulations for the management of urban heat at canyon scale will need to consider the particularities of facades on a case-by-case basis when determining level of detail required for the input geometry. Further research is required to better understand canyon geometry effects such as canyon orientation, aspect ratio and the volumetric influence on internal heat storage in buildings. The investigation was carried out in association with ICube Laboratory (UMR 7357 CNRS-Université de Strasbourg), for the 2012 Geomatics Synthesis Project.

Keywords. 3D modeling, urban heat, urban canyon, thermal imaging

1. Introduction

The urban heat island (UHI) effect is an anthropogenic phenomenon of interest to urban climatologists, health professionals, urban planners and architects. Urbanization tends to alter micro and macro-climatic conditions such that temperatures in urban areas fluctuate differently than non-urbanized areas. For cities of warmer climates, this could potentially add several degrees to the experienced warmth in a city especially at night, possibly creating discomfort and unhealthy living conditions.

There are also concerns that the entrapment of heat by cities increases the attenuation of local air pollutants, leading to public health and other environmental effects.

Understanding the UHI phenomena warrants knowledge on how urban morphology influences heat entrapment, retention, and generation at the street (micro) and city-wide (meso) scale. This would inform how cities are built and arranged, and with which materials. UHI research in the urban canopy (from ground to average height of rooftops) investigates the flux of heat from building faces and the ground, which have been simulated in 3D using models such as LASER/F [1].

The original purpose of LASER/F was to generate more precise estimates of heat fluxes for an entire urban area to make air pollution estimates. Early applications used a simple 3D representation of urban canyon geometries and materiality to determine the influence of urban canyons on the overall heat generated in an urban area. Here one urban canyon acts in a collection of canyons within a city and the details within the urban canyon are not considered as important as its overall contribution to UHI.

LASER/F takes as an input (i) simplified 3D geometry of a street canyon and (ii) meteorological conditions (air temperature, relative humidity, air pressure, wind speed and direction) to calculate radiative, conductive, and convective fluxes at canyon surfaces over time with reasonably accurate results. However, with increasingly detailed 3D geometries for urban areas, it becomes possible to test model sensitivity to changing geometric levels of detail.

This study examined whether a higher level of detail in geometry and materiality would affect the simulation accuracy within an urban canyon. The hypothesis was that the level of detail improves accuracy. The shape, orientation, and materiality of building facades have a meaningful effect on the flux of heat within a canyon. If true, it follows then that 3D geometry complexity also influences the simulated fluxes at the top of the canyon, and therefore its overall contribution to UHI in an urban area. However, with fixed computational power, the computation time is negatively affected.

The data to undertake the study was obtained from three measurement campaigns. The detailed 3D geometry of the urban canyon was generated by the Faculty of Architecture of Strasbourg in July 2001 using photogrammetry and converted to an AutoCAD file. The meteorological data was obtained from a two-week measurement campaign from September 9-22, 2012 on a nearby rooftop at the University of Strasbourg main campus. Finally, thermal images of two canyon façades were taken hourly over 24 hours on September 15, 2012 and used to validate the LASER/F simulation results.

On one hand, the research results inform to what level of detail 3D geometry should be prepared in order to achieve satisfactory results with LASER/F that balance accuracy, precision and time for an urban canyon UHI analysis. This leaves the LASER/F model untouched. On the other hand, it provides a critical window by which to examine how such simulations could be improved to address UHI questions at the micro-scale.

1.1. Urban Heat Island and Surface Energy Balance Equations

According to U.S. Environmental Protection Agency [2], the UHI effect is when "...urban and suburban areas experience elevated temperatures compared to their outlying rural surroundings; this

difference in temperature is what constitutes an urban heat island." While studies in UHI can be based on the surface or air temperature, urban canopy layre (UCL) studies tend to report on air temperatures [3]. With LASER/F, this study has been able to report on surface temperatures at the UCL.

Based on the literature by Oke [4], Rasheed and Robinson [5] and Kleerekoper et al. [6], it seems that the strength of the UHI phenomenon is strongly dependent on geographic location, size and the meteorological conditions of the urban area. This means that urban morphology has a significant role to play in UHI mitigation strategies since cities cannot be moved nor climates changed.

UHI is a combined effect of heat generation (by anthropogenic sources), heat retention (by increased surface area of materials with low albedo and high heat storage capacity, reduced sky views, lower latent heat flux due to reduced vegetation, and reduced turbulent heat transport), and heat entrapment (by canyon geometry or down-reflected radiation by greenhouse gases). Consequently, surface temperatures in urban areas are warmer at night as heat is released slower than in non-urbanized areas (Figure 1). UHI could be mitigated by increasing surface albedo, sky view factor, vegetation and flowing water bodies throughout the city.

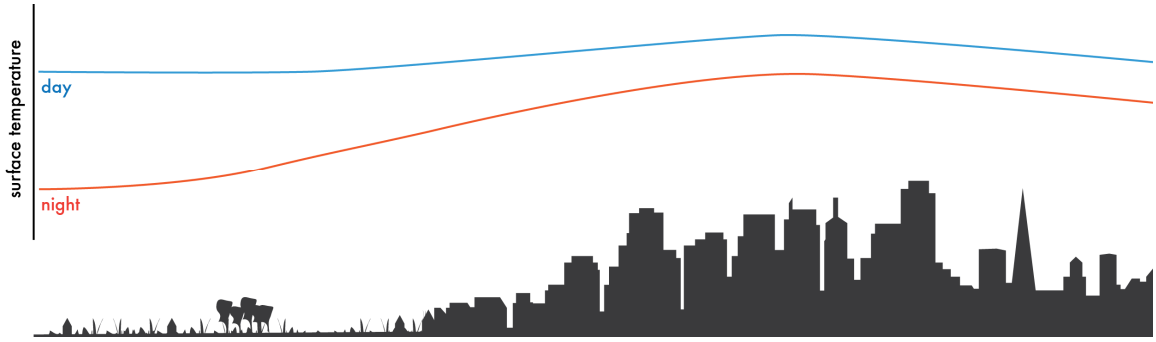

Figure 1. UHI is more pronounced at night than during the day

The energy balance at the UCL is mainly controlled by micro-scale, site-specific characteristics and processes [7]. If scale decreases, spatial variability decreases, and the influence of surface details are increasingly generalized. Heat exchange models between the UCL and the above urban boundary layer (UBL) will undoubtedly be affected by the calculated heat at the UCL. The effect of geometric scale on accurate calculations at the UCL is the subject of interest in this study.

An overview of radiative processes in the UBL is given by Oke [8]. Incoming short-wave solar radiation is partly back-scattered back by the atmosphere and partly transmitted towards the surface. Transmitted radiation can be either absorbed by surfaces or reflected back to the atmosphere. Absorbed radiation is then slowly emitted back to the atmosphere as long-wave radiation (warming the air) that can also be re-absorbed by other surfaces (warming of the urban surroundings). The fraction of the incoming short-wave radiation to the UCL must be balanced with all energy exchanges in the urban canyon.

The basic surface energy balance equation (Equation 1) accounts for all exchanges of energy on a specific surface by simulating all radiative, latent, sensible and surface heat fluxes that act in the UCL [9]. The assumption is that the surface is homogeneous in its radiative, thermal and geothermal properties [10]. If not, then the surface must be fragmented into different elements so that the surface energy balance can be calculated for each element, which is possible in LASER/F.

(1) $Q^* = K^* + L^* = Q_H + Q_E + Q_G$ [Wm^{-2}]

In Equation 1, Q^* represents the net wave radiation describing the sum of the net short-wave (solar) radiation K^* and the net long-wave (infrared) radiation L^*. The Q_H is the sensible heat flux (convective and conductive), Q_E the latent heat flux (evaporative), and Q_G is the (sub)surface or ground heat flux (heating and cooling).

Looking at the short wave component, K^* (Equation 2), S is the direct solar radiation and D is the diffuse solar radiation, α the albedo (reflecting power of a surface), and ζ_{short} is the absorptivity of short-wave radiation of a surface. The long wave component, L^* (Equation 3), is composed of $L\downarrow_{sky}$, the sky emitted long-wave and $L\downarrow_{env}$, the reflected long-wave radiation less the surface emitted radiation (as described by emissivity compared to σ, the Stefan-Boltzmann constant for a black body).

(2) $K^* = K\downarrow + K\uparrow = (S + D) + \alpha K\downarrow$, where $\alpha = (1 - \zeta_{short})$

(3) $L^* = \zeta_{long} L\downarrow - L\uparrow = (L\downarrow_{sky} + L\downarrow_{env}) - \sigma \in_s T_s^4$

Thus the surface energy balance equation can be rewritten in a form that is solely dependent on the surface temperature (Equation 4) and is calculated at each time step for each surface area in LASER/F.

(4) $K^* + L^*(T_s) + Q_H(T_s) + Q_E(T_s) + Q_G(T_s) = 0$

The electromagnetic terms in the surface energy equation are balanced by the non-radiative fluxes. In LASER/F these fluxes are calculated by using the following methods:

- Sensible heat flux: determined by using methodology described in [11]. The thermal performance of roofs, is extended to other materials in LASER/F.
- Latent heat flux: the Penman-Monteith method as described in [12]
- Ground heat flux: the Fourier's law of heat conduction is used [13]

1.2. Air and surface temperatures in urban canyons

Urban canyons are formed by the organization of cities into blocks and streets, with buildings generally being built up to the block edge. Oke [14] defines a basic urban canyon to be made up of the following components: (i) the floor, (ii) the walls and (iii) the air mass in between the walls. The sky above could be considered a fourth component, as it is a sink for outgoing terrestrial long-wave radiation (Figure 2). The idealized, or `regular', urban canyon is symmetric about the centre of the road and consists of two long uniform volumetric blocks with flat roofs, flanking either side of the canyon floor. The materials of the walls would behave homogeneously (heat capacities, albedo and emissivity).

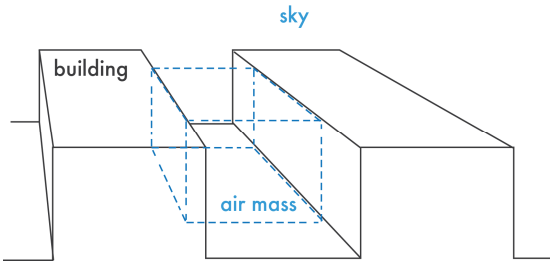

Figure 2. A conceptual diagram of an ideal urban canyon (adapted from [14]).

The literature suggests that there are three overarching features to characterize an urban canyon with respect to impact on micro-climate: geometry, surface properties and vegetation (Figure 3). In this research project, of concern was geometry.

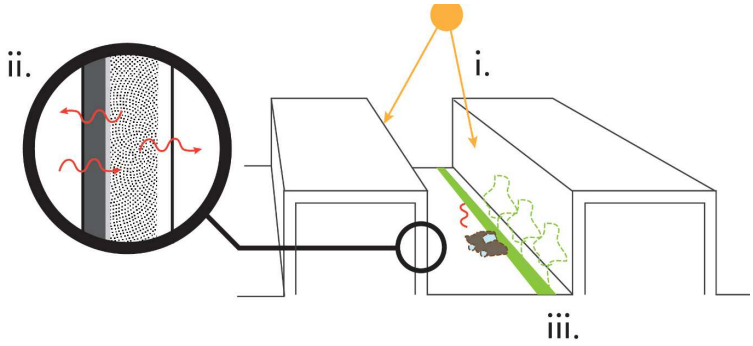

Figure 3. Three overarching features that characterize an urban canyon are (i) canyon geometry, (ii) surface properties, and (iii) street vegetation (for latent heat) and furniture (inducing mechanical air turbulence).

Urban canyon geometry (Figure 4) is described by the (1) orientation (cardinal direction), (2) aspect ratio and (3) sky view factor (SVF). The orientation of the canyon describes the direction of the street in relation to a referenced north and affects the coverage and incidence angle of direct solar radiation and solar gain by canyon surfaces [15]. The aspect ratio is the ratio of canyon height to width (H/W) and is related to the SVF. Aspect ratio and SVF generally affect the amount of heat dissipation and air turbulence patterns.

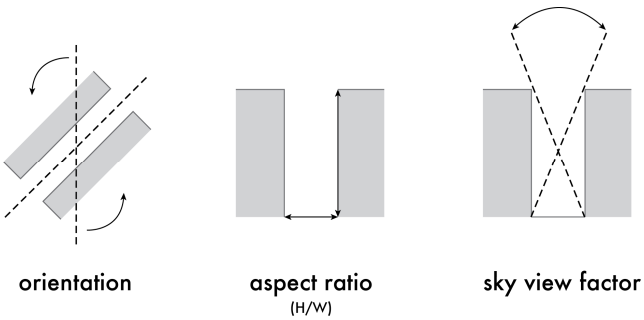

Figure 4. The geometry of an urban canyon can be described by orientation, aspect ratio, and sky view factor.

The SVF is an index (between 0 and 1) of the sky visibility from a given point in the canyon. This is important because the sky acts as a net heat sink from the canyon. In general, a smaller SVF (a narrower canyon) reduces heat escape through the top of the canyon. On the other hand, smaller SVF occludes canyon surfaces from receiving direct solar radiation creating a net cooling effect (Bourbia and Boucheriba 2010). The influence of shadowing versus heat entrapment on air tem-

perature depends on the street orientation [15]. It seems that SVF is more influential for north-south oriented streets where shadows cast by tall buildings are prolonged.

There is also a net cooling effect of wind. When the wind is on an oblique angle to the canyon orientation, generally the wind spirals through the canyon, which can be an effective ventilation mechanism, but this depends on the strength of the synoptic winds. A canyon with a low aspect ratio observes isolated roughness flow of cross-winds (perpendicular to the canyon orientation), where the air flow does not become trapped in the canyon [16]. Higher aspect ratios with a cross-wind creates a major eddy formation toward the windward side and a minor counter circulation pattern on the leeward side, thereby entrapping air pollutants on the street [17,18,19,20]. Asymmetric configurations (termed step-up or step-down, with respect to the direction of the cross-wind) show similar eddy formations.

The heating of canyon walls also stimulates convective heat exchange resulting in rising, buoyant air. With uniformly heated canyon walls, a strong positive correlation between air temperature and aspect ratio was found [18]. This suggests that increasing buildings heights has a net warming effect on canyon air temperature. A profile of the pollutant concentration by convective air movement depends on the surface that is being heated (leeward, windward, or ground), which changes during the day as the sun moves across the sky (Figure 5, [21]). The contribution of convective heat exchange to the overall energy balance becomes increasingly important with decreasing thermal resistance of the facades [22].

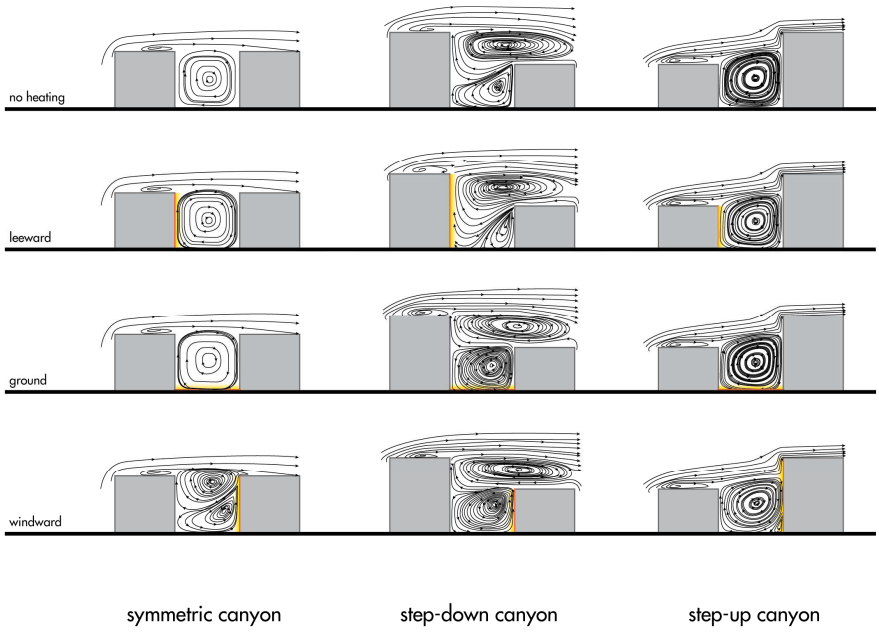

Figure 5. Expected vertical wind profiles of various canyon aspect ratios and surface heating scenarios – Given a cross-wind of 2 m/s, different heating scenarios will change the circulation pattern in the canyon by creating buoyant air (adapted from [21]).

Vegetation and street furniture, also induce complex ground turbulence [23]. Tree-lined streets add shading, but it also increases latent heat flux through evapotranspiration (by being a convective heat sink). This can attenuate some heating effects due to canyon geometry alone. However, the effectiveness depends on the tree variety and leaf temperature and therefore geographic location and season [24]. Unfortunately, it was not possible to model the effects of trees and street furniture in this study.

2. Methods

2.1. Site description

The urban canyon chosen for this research project is Rue de l'Argonne, in Strasbourg, France, located in the city center of Strasbourg, (48.33˚N, 7.38˚E), a city in the Alsace region with a population of nearly 280,000 inhabitants (Figure 6). The average height of adjacent urban blocks around the canyon are between 5 and 7 storeys. The canyon represents a typical city center street and the buildings are used for mixed residential-commercial use, and is located half-way between two canals that are about 700m east and west respectively.

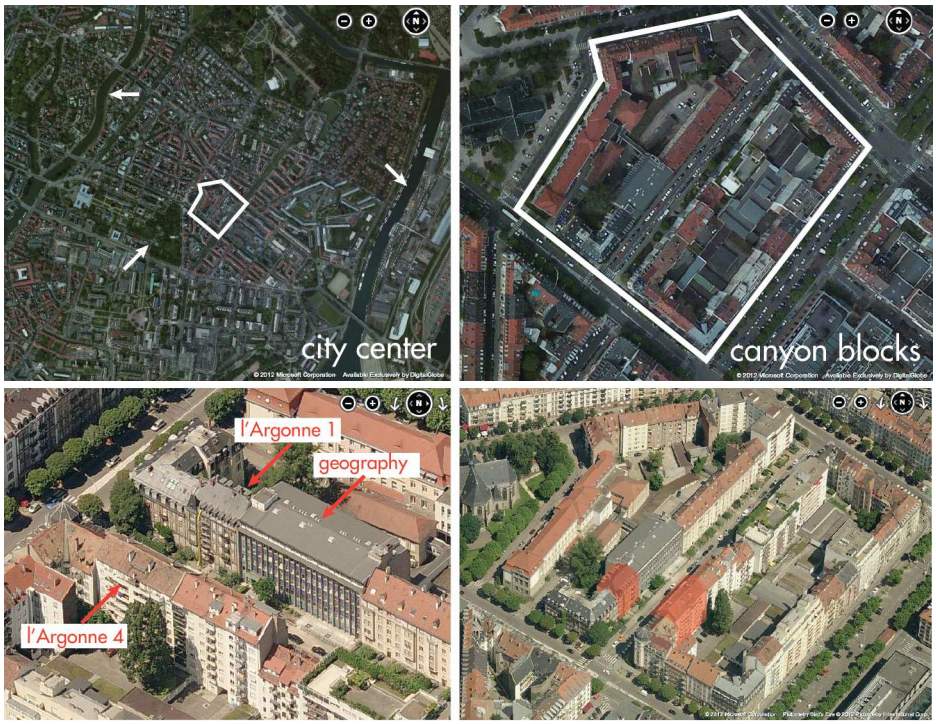

Figure 6. The urban canyon (Rue de l'Argonne) from a birds-eye and isometric view.

This urban canyon is roughly 170m long, 20m wide (from facade to facade), and 15-20m high, depending on the individual buildings. Therefore the aspect ratio (H/W) is between 0.75 and 1. The street can be considered as a regular symmetric urban canyon. It is oriented at about 35˚ from the north, which means the east-facing side of the street is illuminated in the morning and the west-facing side in the afternoon. Due to its orientation, the southern end of the canyon is illuminated longer than the northern end throughout the day (morning shadows in the northern end), although the difference was not measured directly.

Late August and early September is a seasonal transition period between summer and autumn. The average daily high temperature is between 21 and 24 ˚C and lows between 10 and 13 ˚C. The average precipitation is about 50 to 80 mm in this season. This coincides with the annual precipitation peak, but with only 10 to 12 days of precipitation. Relative humidity at this time was measured at around 20%. During field measurements, the sunrise was around 07:10 and sunset at 19:40 and there was no precipitation. Wind in the area around the canyon was blowing from differing directions depending on the day at an average of 1.4 m/s.

The building materials that are used on the surfaces of the canyon are typical for most urban areas. Facades typically feature stone bricks and concrete with glass windows. There are also buildings with ceramic tiles on all or part of the facades. Some buildings use steel framed balconies, or balconies that share the same surface material as the wall (e.g. respectively 1 and 4 Rue de l'Argonne). The dark traffic road is probably paved with asphalt concrete, although this was not verified.

The buildings on both sides are set back about 5m from the edge of the traffic road. Within this setback there is a front garden for nearly every building along the street, consisting of a few trees (covering some the façades), bushes and shrubs no more than 2.5m in height. Little grass is present along these vegetation strips. A single row of on-street parking flanks the traffic roads and is consistently occupied with vehicles.

2.2. Data preparation

As with every model, LASER/F is an approximation of natural processes, which in this case are the surface energy exchanges. The net radiation balance is the term that is simulated in LASER/F using parametrizations in combination with measured quantities as forced input to compute radiant terms. The model uses 3D geometry and local meteorological conditions as input that were collected in two separate measurement campaigns.

2.2.1. Meteorological data

The LASER/F model requires a number of meteorological descriptions in the form of a so-called forcing file. A temporary meteorological station was set-up 15-20m above the ground about 650m south west of the canyon and measured air temperature (K), relative humidity (%), wind speed (m/s), wind direction (degrees), direct/diffuse/terrestrial irradiance (W/m^2). Since the irradiance measurements were taken every two minutes and the air measurements every fifteen minutes, the time interval of the data in the forcing file was set to fifteen minutes.

2.2.2. 3D Geometry and simulation scenarios

A detailed AutoCAD model of the Rue de l'Argonne in Strasbourg was generated by the University of Strasbourg Faculty of Architecture in July 2001 using photogrammetry (Figure 7). The acquisition was done from within the canyon itself, meaning that there was no detailed 3D information on the facades at the back of buildings. The level of complexity in the model is also inhomogeneous throughout the canyon so it was decided to select two relatively detailed opposing facades for testing geometry effects (1 and 4 'Rue de l'Argonne, Figure 8). It was not feasible to simulate the full canyon in LASER/F with the highest geometry complexity due to lengthy computational time.

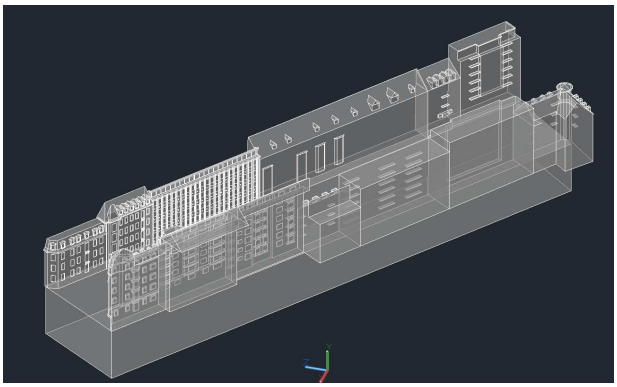

Figure 7. Visualization of the original 3D geometry obtained by the University of Strasbourg Faculty of Architecture showing the higher level of detail in façade design on the left than on the right end of the canyon.

Figure 8. Rue de l'Argonne 1 (above) and Rue de l'Argonne 4 (below) above) façade details and 3D model.

To be able to convert the AutoCAD model into the LASER/F .geo file format the .dwg file was converted to an ASCII Scene Export (ASE) file using Autodesk 3DS Max. This is done separately for each building/object in the 3D scene. With the same program the different faces are given different colours (representing materials). A Python program is developed to read the ASE files (get the vertexes, faces and materials from the file), convert this data to the .geo file format syntax and to write a Virtual Reality Modeling Language (VRML) file for visualization of the scene.

Since radiation and heat simulations are computationally expensive, the influence of distinct geometric features such as windows, balconies and roofs were examined individually rather than with a compound approach to increasing geometric level of detail. The input files of seven 3D geometry scenarios described below (Figure 9) were prepared and compared against a base case (simplest 3D geometry of the canyon) to determine the sensitivity of LASER/F to geometric details. The changes in the geometry were only applied to the two buildings of interest, but the entire canyon was run in each simulation. The seven geometry scenarios were:

1. base case: Extruded building footprints to roof base height (without roofs)
2. base case + simple roofs: extruded footprints with simple roofs
3. base case + complex roofs: extruded footprints with the originally provided roof complexity
4. base case + windows: the shape of the windows are projected on the extruded blocks
5. base case + balconies: the geometry of the balconies is connected to the extruded blocks
6. complex case: the full complexity of the original 3D geometry provided
7. complex case + vertex welding: the complex case simplified by vertex welding technique

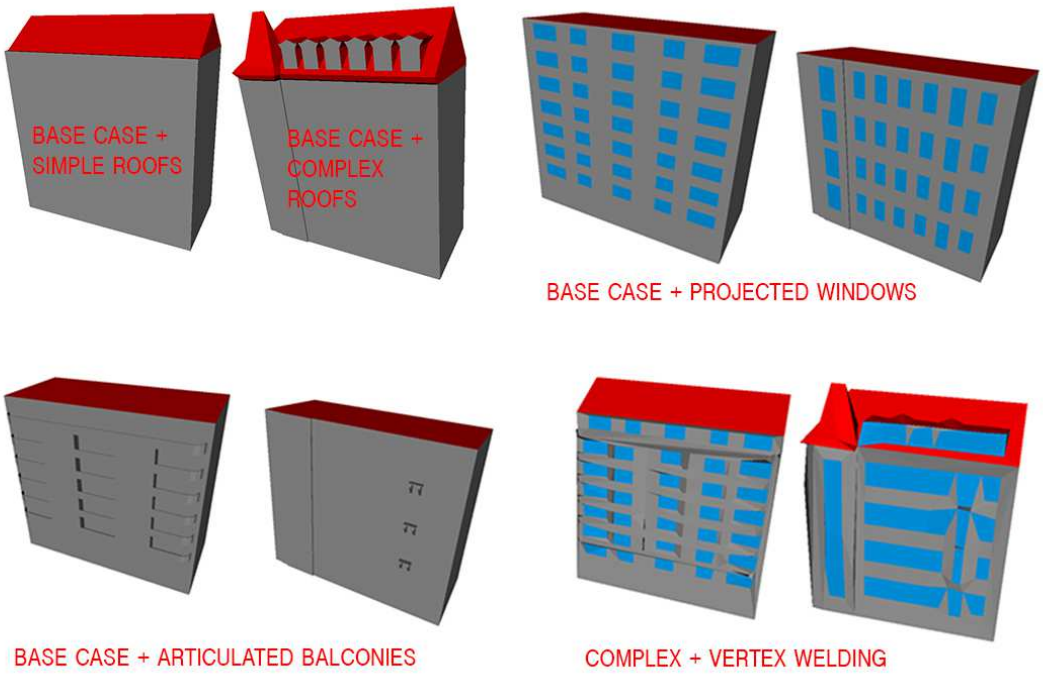

Figure 9. Visualization of five of the geometry cases for the two buildings of interest.

2.2.3. Thermal imagery and calibrations

Seven ground positions were used to measure temperature of the buildings of interest, with an additional position on the second floor of the Faculty of Geography to capture road images when time permitted (Figure 12). The measuring distance to the façade was approximately 19m. Each image captured an area of 8.4 x 6.3m and multiple images were required to capture the entire facade. For the ground positions this results in 12 images of 1 Rue de l'Argonne and 20 images for 4 Rue de l'Argonne per epoch.

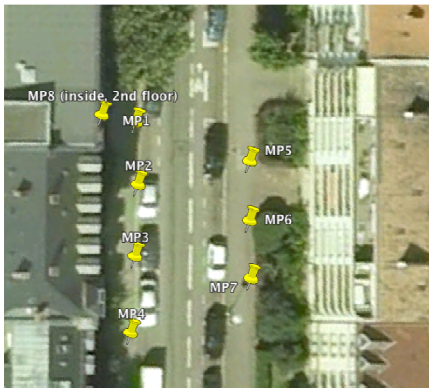

Figure 12. Measurment points (MP) for the 24-hour thermal imaging campaign.

Measurements were taken over 24 hours at 1-hour intervals to capture the surface cooling and warming trends. Measurements at night (21:00-06:00) were set at a 3-hour-interval since no hourly changes were expected. A FLIR SC665 thermal camera was used. It was equipped with a microbolometer which does not require cooling, and was limited to the spectral range of 9-11 μm where the surface emissivity variation is minimized and the transmissivity of the air is high.

Lens distortion coefficients and focal length in pixels were estimated for rectifying all thermal images using the Matlab camera calibration toolbox and a calibration algorithm of the TU Delft (Ben Gorte, Optical and Laser Remote Sensing). The estimated focal length (1528 pixels and 1523 pixels respectively) served as an indicator of whether the focal length stated by the supplier is correct, and was useful as a guide for the collinearity equations (for comparing the thermal images to the LASER/F results).

2.3. LASER/F Model and running 3D geometry scenarios

LASER/F simulates terms of the energy balance at a high spatial resolution and in a full 3D environment. The simulations are done on a scene that consists of objects. Objects can be buildings, terrain or street furniture that are built from different faces with different material properties. Material type is parametrized within LASER/F by two different tables: material properties and material structure. The material properties table contains the direct and diffuse reflectivity, emissivity, conductivity, specific heat, density and refraction index for each material type.

The object faces are further fragmented into a triangular mesh where the energy balance equation is solved at each mesh center point. The maximum size of the triangles is set to be 5 m^2, which is a balance between computation time and level of detail. The model uses a hemisphere to simulate the sky, which needs to be fragmented as well. For the simulation the sky is divided into 256 faces. For each of those faces, it needs to be determined to which geometry fragments these have free line of sight. For this, a SVF and a form factor are introduced, which both evaluate the visibility of all the sky meshes for each geometry mesh [1].

2.3.1. Baseline determination

Two additional model calibrations had to be implemented with the 3D geometry in order to better represent the actual site conditions (Figure 13). These were determined by a series of preliminary tests. The first was whether to open or close the canyon with additional geometry. An open canyon poorly represented the urban setting whereas the canyon is surrounded by other streets and adjacent buildings. Adding wall category of ‘ground’ in the approximate locations of adjacent street walls

accounted for up to 5K temperature difference especially in the evening hours. Also, the presence of vegetation in the canyon probably contributes to the latent heat flux. In this case, modeling both sides of the street with 5m grass strips (according to Google Earth image interpretation) accounted for up to 2K temperature difference.

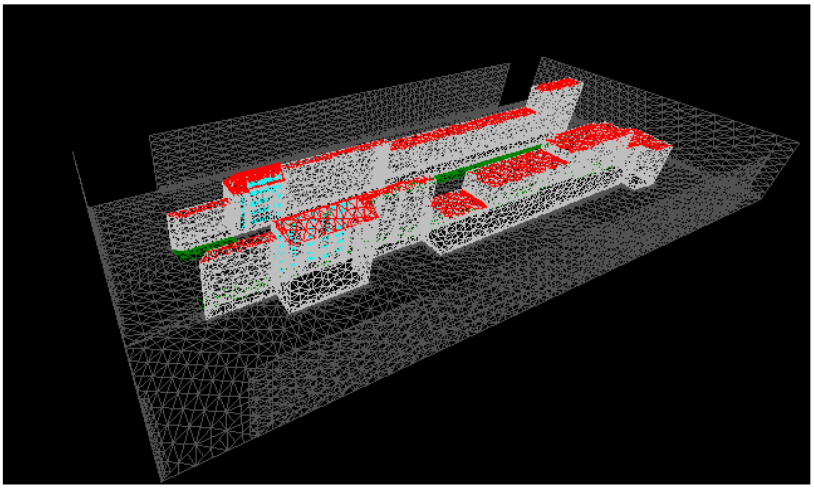

Figure 13. Visualization of the triangulated mesh created by LASER/F using the base case + full complexity for the two buildings of interest, illustrating the locations of the closed canyon walls and grass strips.

2.3.2. Running each geometry scenario

For each 3D geometry scenario, the simulation was run at a time interval of fifteen minutes specified in the forcing file. The simulation required a stabilization period of one day to get the microclimate into a state of equilibrium (allowing the soil and building interiors to be heated). The internal heat storage and inertia of heating the building is evaluated based on building volume. This volume is calculated from the footprint of the roofs and the associated height. It does not take into account details on the walls of the buildings. However, the authors' note that the original 3D geometry provided for this study did not model building volume accurately.

The surface temperatures for every mesh is computed in two steps. First, all flux terms are computed and serve as input for the energy balance equation. Using the flux terms, the surface temperatures (T_s) are calculated. This continues iteratively until the temperature difference is less than 0.01 K. Next, the radiant exitance can be calculated using the surface temperatures iteratively until the iterative radiant exitance difference of 1 W/m^2 is reached. Thus, the final surface temperatures can be calculated for each triangular mesh center point (with an associated x,y,z coordinate) per epoch.

2.4. Validation by thermal imagery

An object with a temperature above absolute zero emits energy in the form of radiation that can be sensed remotely. The detector in the thermal camera works on the basis of changes in temperature of the detector, which is induced by the incoming photons that alters the current, voltage or conductivity within the detector. This is recorded as the temperature of the target. However, all impinging radiation detected by the thermal camera stems from the emitted radiation from the target object, the radiation reflected from the target and the radiation emitted from the atmosphere between the camera and target. Thus the temperature recorded by the camera does not equal the actual surface temperature of the target and images should be corrected.

Since the recorded measurements could not be decomposed to find actual surface temperature, radiance exitance was calculated from the thermal measurements using Stefan-Boltzmann's law and compared with radiant exitance from LASER/F (calculated as the sum of radiant emittance and reflected radiation). In this case no error sources, like emissivity or reflected radiation, had to be accounted for.

2.4.1. Projection of 3D points to 2D thermal image

LASER/F provides a visualization in which the calculated radiances are mapped onto the 3D surfaces. It also provides an output containing the (x,y,z) coordinates of the triangle mesh center point. These 3D simulation results from the seven geometry scenarios were compared against the rectified 2D thermal images by essentially projecting the 3D vertices and centerpoints onto a 2D raster image domain.

To project a 3D point to the 2D thermal image, the camera rotation parameters (ω,κ,ϕ) the camera translation parameters (X,Y,Z) and the focal length *f* of the camera were used to solve the collinearity equations. A space resection method was used assuming that the camera position remained constant at all measurement epochs. The output was an (x,y) position which indicated the location of the 3D point in the 2D image. This coordinate was rounded to the nearest integer and mapped onto the corresponding thermal image. Points projected outside the boundaries of the image were removed.

To project the triangles onto the 2D image, a list of triangles corresponding to the thermal image were first filtered to remove triangles representing buildings sides and backs. This was accomplished using a manually defined bounding box. Triangles with center points inside the bounding box were selected and removed. Then triangle vertices were projected into the 2D image domain and snapped to the raster image grid. The triangle vertices were connected to form edges, filled in with pixels, and given the radiant exitance value from the LASER/F simulation.

Additional thermal image filtering was required to remove complexities and pixels that were not of interest. Clear sky was easily removed by filtering out temperatures below 223K. Areas where vegetation was occluding the façade were masked out first in the 3D model and projected onto the 2D simulation image. Windows were also masked out as the measured temperature contained too many sources of error that could not be resolved.

For a fair comparison between the projected 2D LASER/F simulations and the thermal images, the thermal image was also reconstructed according to the triangle geometry in the projected LASER/F image so that a triangle-by-triangle comparison could be made. The value of each triangle was the average temperature of the pixels of that triangle. Finally, the 2D LASER/F image was masked by the filtered thermal image such that every facade pixel corresponded between images. In this way, a set of projected images for each building of interest was produced for each geometry scenario for every measurement epoch. Figure 14 visualizes the preparation of the comparable imagery.

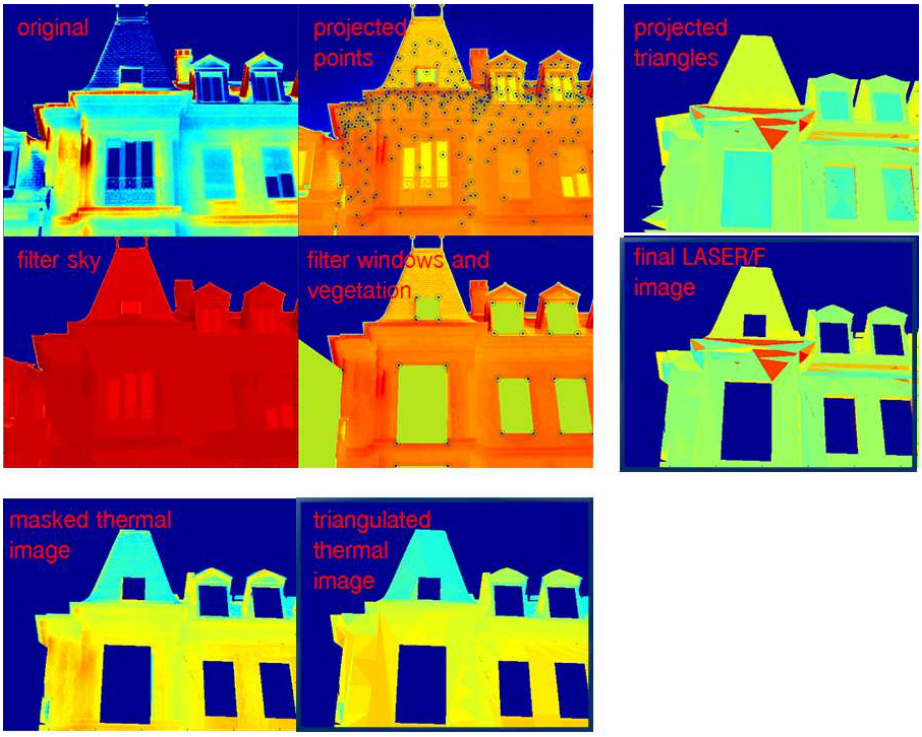

Figure 14. This figure uses one of 12 images taken of 1 Rue de l'Argonne façade to demonstrate the image processing method. Thermal images were used to define the 2D image domain wherein the 3D LASER/F results were projected (points and triangles). Additional filtering and masking of unrelevant and complex pixels followed. The final LASER/F image and triangulated thermal image were used to validate the LASER/F results.

2.4.2. Coarse RMSE comparison

For statistical comparison between the simulated and measured radiant exitances, a students t-test was ruled out because the skewed distribution of exitances from the simulation results while the measured exitances was normally distributed. Instead a coarse comparison of RMSE values was used to validate the simulation results. In this approach, for each geometry scenario, for each building façade, and for the measured and simulated 2D images, measured exitance values per triangle for every epoch was stored in a single vector. This way, the RMSE value was obtained for each geometry scenario for every epoch through a single equation (Equation 5) where *m* and *s* are the measured and simulated pixels respectively and *n* is the number of pixels in each vector. This means that each case of geometry complexity has only one RMSE value.

$$(5)\quad RMSE(m,s)=\sqrt{\frac{\sum_{i=1}^{n}(m_i-s_i)^2}{n}}$$

The error vectors were also investigated. The error vector of each complexity scenario consisted of the differences between corresponding pixel values of the measured and simulated vectors and described how well the model fit the measurements in each simulation scenario. The histogram of these vectors should follow Gaussian distribution with zero mean and described the precision of the model in different epochs, since the standard deviation of residual vectors can be estimated using the histograms.

2.5. CFD simulation

In LASER/F, the assumed vertical wind profile is exponential and without consideration of the frictional forces of the canyon surfaces. Furthermore, the profile is uniform throughout the canyon, which is an oversimplification according to many urban canyon studies. The model that is used to make the critical assessment of this is the Computational Fluid Dynamics (CFD) model developed by the TU Delft Transport Phenomena group. The base case of the canyon was used to simulate the turbulence of air through the canyon, and to extract a vertical wind profile between the buildings of interest (1 and 4 Rue de l'Argonne). Even without the incorporation of thermal equations into the CFD model, the simulation was expected to give a general impression the air turbulence through the canyon, highlighting the difference with the simplification of wind in LASER/F.

The CFD model required 3D geometry as rectangular objects and meteorological forcing conditions, namely the initializing wind speed and direction. The wind parameters used for this simulation was taken from September 15th, 15:00, where the wind speed was 2.25m/s at a direction of 33.67°. This corresponded to the warmest hour of the day where the most turbulent fluxes are expected. The 3D geometry included two street walls that flanked the ends of the canyon similar to the LASER/F baseline geometry. From the model, it was possible to extract wind speed, turbulent kinetic energy (tke), tke dissipation, and air temperature in 3D. Thus it was possible to extract horizontal and vertical wind and temperature profiles at any location in the canyon.

3. Results

3.1. Coarse RMSE comparison

When the RMSE values are averaged over all epochs for each geometry scenario, no drastic differences are noted for both buildings. However, the simulation time does increase significantly. The simulation time for the complex case is almost 9 times longer than for the base case while the complex case is only slightly more accurate than the base case (Figure 15). This confirms the hypothesis that more complex geometry increases simulation time, with a constant computational capacity, because there are be more triangular meshes introduced in the model. Scaling effects on error were not considered in the analysis.

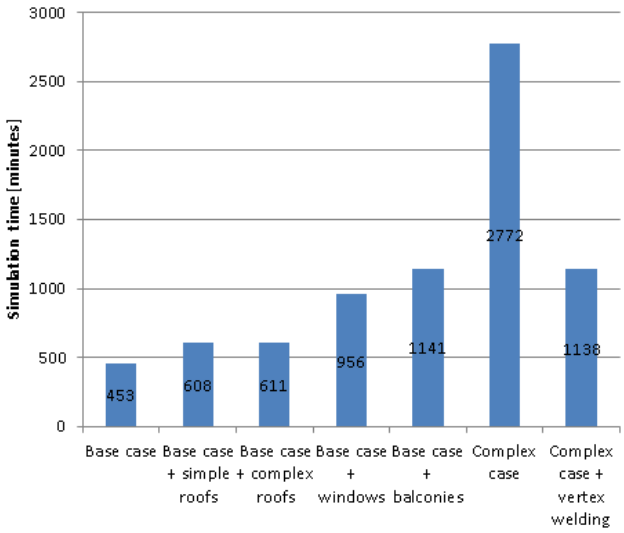

Figure 15. Graph showing computation time for each geometry scenario, in minutes.

It is notable that the RMSE for the base case + balconies of building 1 was around 5-10 W/m^2 lower than all other geometry scenarios. This might be because the surface area of the balcony is a significant geometric addition to the base case compared to building 4 where balconies are smaller and made of thin steel rods. Also for both buildings, the highest RMSE value was the base case + windows, which is likely because the values for the windows were masked out in the thermal images (Table 1).

Geometry scenario	RMSE building 1 (W m^{-2})	RMSE building 4 (W m-2)	Simulation time
Base case	45.84	48.85	7h 33min
Base case + simple roofs	46.3	44.25	10h 8min
Base case + complex roofs	42.85	44.59	10h 11min
Base case + windows	46.93	51.29	15h 56min
Base case + balconies	36.87	43.39	19h 1min
Complex case	40.75	44.59	46h 12min
Complex case + vertex welding	44.68	45.52	18h 58min

Table 1. Overview of simulation time and RMSE values over all epochs for both buildings and each geometry scenario.

3.2. Descriptive RMSE comparison

The effects of geometry complexity are different over time for building 1 and 4 because of their different positions in the canyon and thus different illumination durations. For building 1 (Figure 16), the lowest overall RMSE values occur for the base case + balconies which ranges from approximately 4 W/m^2 to 65 W/m^2 while the largest RMSE values are for the complex case derived from vertex welding (16 W/m^2 to approximately 85 W/m^2). The diurnal difference between these two cases is large. This suggests that the balconies for building 1 have a meaningful effect on the accuracy of the simulation and should be modeled.

Examining the temporal exitance graph of 4 Rue de l'Argonne shows that exitance varies from 5 -52 W/m^2 (Figure 17). In terms of geometry scenarios, the results are different from Building 1. Despite having heavily articulated balconies, it did not have the same effect as with building 1. Total surface area could have been compared between base case and complex case to understand this. The simple roofs performed similarly to complex roofs. This is likely because the ‘complex’ case of the roof is still very simple. Again here vertex welding produced the least accurate simulations.

A comparison of the temporal exitance RMSE curves for each of the buildings illustrate the influence of illumination and shading on RMSE. For both curves, the RMSE values increase steeply when directly illuminated by sunlight (around 7:20 to 12:00 for building 1 and 15:40 to 19:00 for building 4) and geometry complexities seem to have the least effect on accuracy. LASER/F performs better during shaded periods and geometry complexity seems to have a noticeable effect on accuracy. This is not surprising since when the irradiance of the surfaces increases, more complex energy exchanges within the canyon also arise. Since LASER/F and the 3D geometry are approximations of such complex exchanges, the RMSE error is expected to increase as the interactions increase.

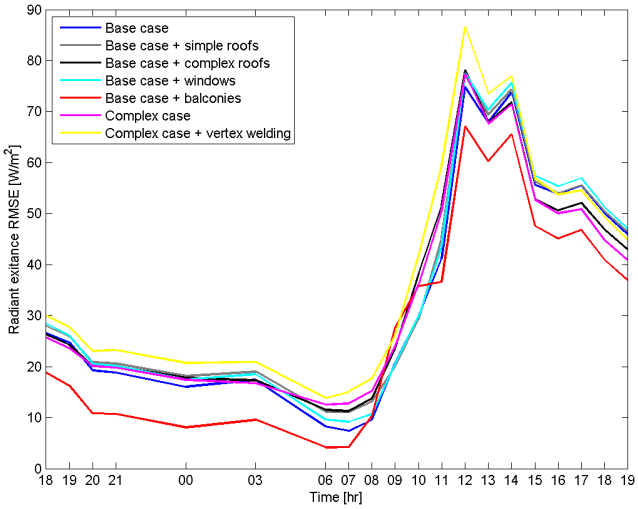

Figure 16. Exitance RMSE for building 1 over a 24 hour period. LASER/F is sensitive to complex geometry of the balcony especially during the warming period.

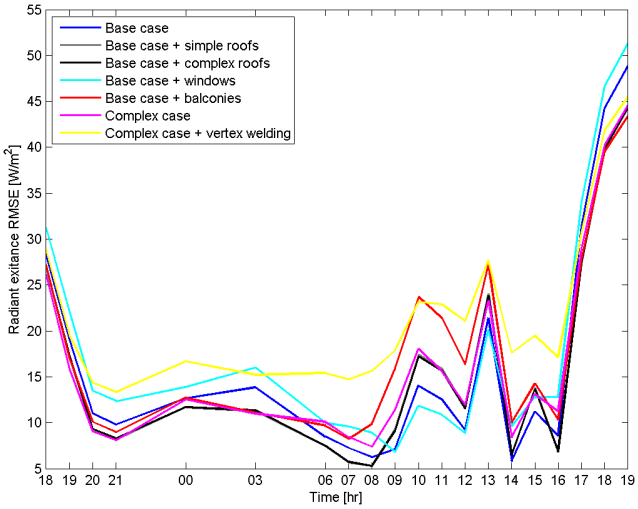

Figure 17. Exitance RMSE for building 4 over a 24 hour period. LASER/F was not as sensitive to balconies or building roof complexity as was with building 1. Prolonged shading during the warming period caused varying RMSE values.

Comparing the measured exitance values to the simulated ones shows that measured values were almost consistently higher than the simulated ones (Figure 18 and 19) probably due to systematically induced errors. This could be because of the model approximations for material properties, surface-air heat exchange parameters, vertical wind profile, and errors in the 3D geometry. For example, the geometry did not model for the full building volumes. Further examination of the input geometry revealed that buildings were closed at the bottom, affecting the ground heat flux and leading to cooler building interiors. Correcting this could reduce the absolute RMSE values.

A comparison of the vertical wind profile in LASER/F and the CFD simulations between the two buildings of interest revealed that wind speeds approximations of LASER/F modeled higher wind speeds than the CFD model (Figure 20), thereby increasing the cooling effect of wind, and possibly explaining the cooler simulated temperatures. There may have been other influential factors that were not part of the input geometry but could explain the differences (such as heat from on-street vehicles and interactions with nearby buildings, vegetation shading and latent heat).

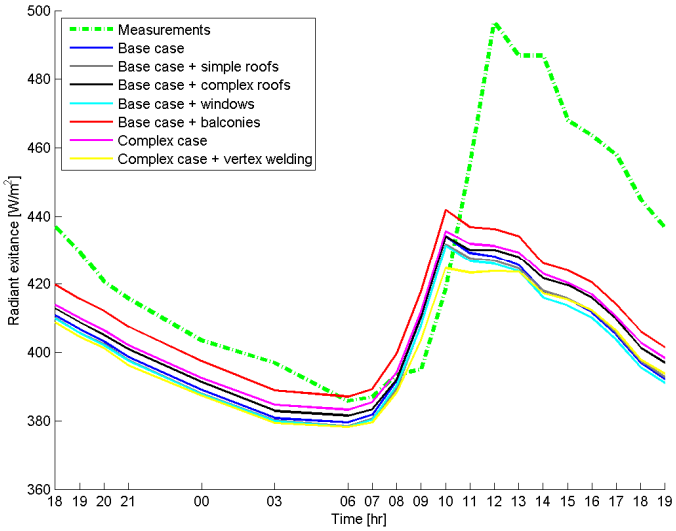

Figure 18. Mean radiant exitance of measurements and simulation scenarios for building 1.

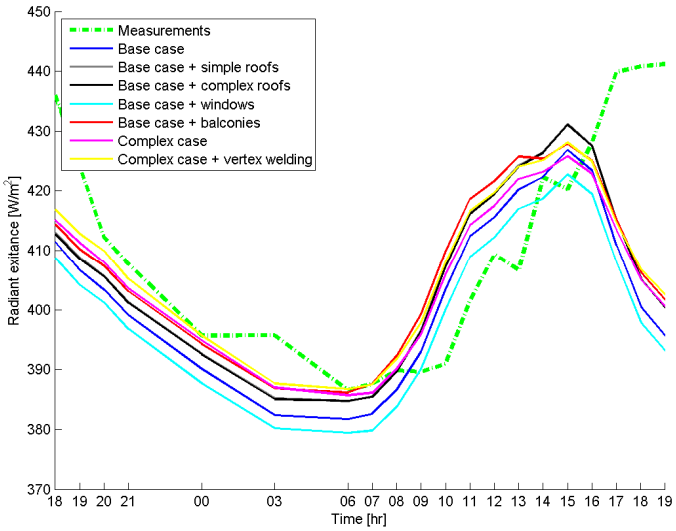

Figure 19. Mean radiant exitance of measurements and simulation scenarios for building 4.

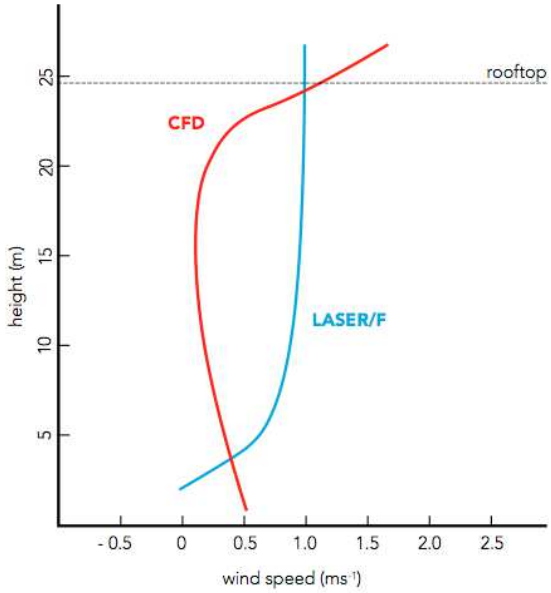

Figure 20. Comparison of the vertical wind profile in LASER/F (blue) and that extracted from the CFD model (green).

4. Conclusions

The initial hypothesis was that adding 3D geometry complexity to the LASER/F model would increase the accuracy of simulated radiative, conductive, and convective flux calculations in an urban canyon. The results indicate that this is not always the case because of the quality of the input data and the importance of particular geometry features (e.g. balconies and windows) to the characterization of a facade. Thus, a 3D urban canyon model level of detail must not be applied uniformly over the entire canyon but consideration must be given to the particular façade articulations of each building. For example, it is not important to model the balconies if without them the facade is still recognizable.

The most complex geometry scenario yielded lower errors than the vertex welding scenario, but was less accurate than when balconies were added, especially for 4 Rue de l'Argonne. Moreover, the lowest RMSE errors occurred at night during the cooling period and the highest during the warming period. Attention might need to be paid to introducing a dynamic parameterization of the model depending on sunrise and sunset hours to correct for this effect.

Simulation accuracy might also be improved by modeling vegetation, street furniture, and parked vehicles as they contribute to the wind turbulence and emitted heat at the surface and could explain some differences during the warming period. The material library and properties could be expanded such that complexity in the façade materiality could also be modeled. The wind profile should also be more realistically approximated with the aid of a CFD model.

The 3D geometry ‘base’ should model the actual building volumes (in this study, some buildings were unusually thin) and be open at the bottom. With respect to the thermal imagery, exact camera positions and orientations should be recorded on-site for each image rather than estimated afterwards to reduce projection errors. Future work might improve upon this work by using a different street, model the adjacent streets, and other orientations and aspect ratios. From an application perspective, the research results are interesting for developing methods to evaluate architectural and urban design interventions on heat fluxes for urban streets or neighbourhoods.

Acknowledgements

Thanks to Georges Najjar, Laure Roupioz, and Robin Faivre of the ICube laboratory at the University of Strasbourg for their gracious hospitality toward the TU Delft team during the two-week visitation, which was an invaluable and memorable experience. Thanks also to Patrick Schrijvers of the Transport Phenomena group at TU Delft for training and allowing us to use the TU Delft CFD model to enhance our analysis.

References

[1] Kastendeuch P P & G Najjar, 2009. *Simulation and validation of radiative transfers in urbanized areas.* Solar Energy, 83(3):333-341.

[2] U.S. Environmental Protection Agency, 2004. *Reducing urban heat islands: Compendium of strategies, chapter 1: Urban heat island basics.* Technical report, U.S. Environmental Protection Agency, Washington.

[3] Mills G, 2009. *Luke Howard, Tim Oke and the study of urban climates.* URL: ams.confex.com/ams/pdfpapers/114519.pdf, accessed September 28, 2012.

[4] Oke T R, 1987. *Boundary Layer Climates.* Methuen & Co., London, 2nd Edition.

[5] Rasheed A & D Robinson, 2009. *Multiscale modeling of urban climate.* In Ecole Polytechnique Fédérale De Lausanne Solar Energy and Building Physics Laboratory. Building Simulation 6:505-512. URL:biblion.epfl.ch/EPFL/theses/2009/4531/4531_abs.pdf, accessed October 14, 2012.

[6] Kleerekoper L, van Esch M & T B Salcedo, 2011. *How to make a city climate-proof, addressing the urban heat island effect.* Resources, Conservation and Recycling 64:30-38. URL: linking-hub.elsevier.com/retrieve/pii/s0921344911001303, accessed October 14, 2012.

[7] Arnfield J A, 2003. *Two decades of urban climate research: A review of turbulence echanges of energy and water, and the urban heat island.* International Journal of Climatology 23(1):1-26.

[8] Oke T R, 1982. *The energetic basis of the urban heat island.* Quarterly Journal of the Royal Meterological Society 108(455):1-24.

[9] Oke T R, 1976. *The distinction between canopy and boundary-layer urban heat islands.* Atmosphere 14(4):268-277.

[10] Wu L, 1996. *An integration of a surface energy balance climate model with TIN and GRID in GIS.* In Third International Conference/Workshop on Integrating GIS and Environmental Modeling, Santa Barbara, CA.

[11] Al-Sanea S A, 2002. *Thermal performance of building roof elements.* Building and Environment 37(7):665-675.

[12] Howell T A & S R Evett, 2004. *The Penman-Monteith Method.* Bushland, Texas: USDA Agricultural Research Service 5646(806).

[13] Incropera F P, DeWitt D D Bergman T L & A S Lavine. *Fundamentals of Heat and Mass Transfer*. Dekker Mechanical Engineering, Volume 6. © John Wiley & Sons.

[14] Oke T R, 1977. *The Energy Balance of an Urban Canyon.* Journal of Applied Meteorology 16(1):11-19.

[15] Takebayashi H & M Moriyama, 2012. *Relationships between the properties of an urban street canyon and its radiant environment: Introduction of appropriate urban heat island mitigation technologies.* Solar Energy 86(9):2255-2262.

[16] Oke T R, 1988. *Street design and urban canopy layer climate.* Energy and Buildings 11(1-3):103-113.

[17] Cai X M, Barlow J F & S E Belcher, 2008. *Dispersion and transfer of passive scalars in and above street canyons: Large-eddy simulations.* Atmospheric Environment 42(23):5885-5895.

[18] Memon R A, Leung D Y C & C-H Liu, 2010. *Effects of building aspect ratio and wind speed on air temperatures in urban-like street canyons.* Building and Environment 45(1):176-188.

[19] Salizzoni P, Soulhac L & P Mejean, 2009. *Street canyon ventilation and atmospheric turbulence.* Atmospheric Environment 43(32):5056-5067.

[20] Vardoulakis S, Fisher B E A, Pericleous K & N Gonzalez-Flesca, 2003. *Modeling air quality in street canyons: A review.* Atmospheric Environment 37(2):155-182.

[21] Xie X, Huang Z, Wang J & Z Xie, 2005. *The impact of solar radiation and street layout on pollutant dispersion in street canyon.* Building and Environment 40(2):201-212.

[22] Cole R J & N S Sturrock, 1977. *The convective heat exchange at the external surface of buildings.* Buildings and Environment 12(4):207-214.

[23] Gayev Y A & E Savory, 1999. *Influence of street obsturctions on flow processes within urban canyons.* Journal of Wind Engineering and Industrial Aerodynamics 82(1):89-103.

[24] Shashua-Bar L & M E Hoffman, 2003. *Geometry and orientation aspects in passive cooling of canyon streets with trees.* Energy and Buildings 35(1):61-68.